ELSEVIER

Nuclear Physics A 703 (2002) 466–488

NUCLEAR PHYSICS A

www.elsevier.com/locate/npe

# Different isotopic composition as a signature for different processes leading to fragment production in midperipheral $^{58}$Ni + $^{58}$Ni collisions at 30 MeV/nucleon

P.M. Milazzo [a,*], G. Vannini [b], C. Agodi [c], R. Alba [c], G. Bellia [c], M. Bruno [b], M. Colonna [c], N. Colonna [d], R. Coniglione [c], M. D'Agostino [b], A. Del Zoppo [c], L. Fabbietti [e], P. Finocchiaro [c], F. Gramegna [f], I. Iori [e], K. Loukachine [c], C. Maiolino [c], G.V. Margagliotti [a], P.F. Mastinu [f], E. Migneco [c], A. Moroni [e], P. Piattelli [c], R. Rui [a], D. Santonocito [c], P. Sapienza [c], M. Sisto [a]

[a] *Dipartimento di Fisica and INFN, Trieste, Italy*
[b] *Dipartimento di Fisica and INFN, Bologna, Italy*
[c] *INFN, Laboratori Nazionali del Sud, Catania, Italy*
[d] *INFN, Bari, Italy*
[e] *Dipartimento di Fisica and INFN, Milano, Italy*
[f] *INFN, Laboratori Nazionali di Legnaro, Legnaro, Italy*

Received 11 September 2001; revised 26 October 2001; accepted 5 November 2001

**Abstract**

We report on the results of experiments performed to investigate the $^{58}$Ni + $^{58}$Ni 30 MeV/nucleon reaction. In midperipheral collisions a massive fragment ($4 \leqslant Z \leqslant 12$) production has been observed. The emission patterns exhibit features consistent with dynamical fragmentation of a neck zone between the interacting nuclei, while in addition and at the same time, the projectile-like and target-like residues are subject to statistical decay. The nature of the fragments produced via the two different mechanisms differ both for what concerns charge distribution and isotopic composition. In particular, neutron rich fragments can be produced in dynamical processes, even if the starting nuclear matter presents a $N/Z$ ratio close to the unity. © 2001 Elsevier Science B.V. All rights reserved.

*PACS:* 25.70.Pq; 25.70.-z
*Keywords:* Heavy ions; Multifragmentation

* Corresponding author.
*E-mail address:* milazzo@trieste.infn.it (P.M. Milazzo).


PII: S0375-9474(01)01337-9

## 1. Introduction

The study of nuclear reactions in the Fermi energy domain (30–50 MeV/nucleon) is one of the major topics of nuclear physics. Different mechanisms have been proposed to explain how the interacting nuclei exchange mass and energy or fuse to form a new structure.

The multifragmentation, i.e., the presence in the exit channel of the reaction of multiplicities higher than 2 of fragments with charge $Z \geqslant 3$ (intermediate mass fragments, IMF), is one of the main de-excitation mode in this energy regime.

In particular, for central collisions, at low energies ($E \leqslant 20$ MeV/nucleon) the nuclear mean field rules and fusion-fission processes are observed, when on the contrary, at high energies ($E \geqslant 100$ MeV/nucleon) the direct nucleon–nucleon scattering produces a complete vaporisation of the system; in the intermediate energy range many IMFs are emitted and this phenomenon has been successfully described by statistical approaches. Similarly, for peripheral collisions, at low incident energies binary energy dissipative processes are observed, and at high energies the collisions are well explained in terms of the participant-spectator models where the overlap region between the projectile and the target fully decouples from the spectators. For this impact parameter regime and in particular for midperipheral collisions, at the Fermi energies many experimental evidences have shown that the formation of a neck-like structure joining quasitarget (QT) and quasiprojectile (QP) can occur. Even in this case the production of IMF (of dynamical origin) is the distinguishing feature.

From the theoretical side the particular form of the nuclear forces leads, for infinite nuclear matter, to an Equation of State (EoS) similar to that of the Van der Waals gas, which is likewise characterised by the existence of a liquid-gas phase transition [1]. Experimental results [2–5] seem to indicate the existence of signals related to a possible liquid-gas phase transition. While some of the results [3,5] suggest critical behaviours of some observables, other data [2,4] rely on the measurement of the temperature of nuclear systems and on the particular shape of the caloric curve. These results agree with predictions of statistical multifragmentation models [6] and suggest that multifragmentation may result from a phase transition near the critical point [7]. However, the processes leading to the formation of neck-like structures can not be described on the basis of statistical approaches and are connected to the dynamics of the collision [8]. Therefore, one of the central issues concerning the multifragmentation process is the interplay between the attainment of the thermal and chemical equilibrium of the excited nuclear matter prior the production of fragments and the dynamics involved in their emission. In this respect the study of the characteristics of the formation and decay of the neck-like structures is of great importance. With the advent of radioactive beam facilities and of high resolution experimental apparatus, the interest has been addressed towards the influence of the isospin degree of freedom, which certainly is an important probe of the dynamical aspects of the formation and decay of the hot nuclear matter in heavy ion collisions. In fact, the nonequilibrium dynamical behaviour of nuclear systems, such as the neck-like structures, can be strongly influenced by isospin effects.

In this sense the mechanism leading to the rupture or to the re-absorption by the collision partners of the neck-like structures has important theoretical implications [9]. In fact, the isospin dependence and the viscosity term of the EoS play a fundamental role in the formation and decay of such a IMF sources.

In this paper we present and discuss data on $^{58}$Ni + $^{58}$Ni midperipheral collisions at 30 MeV/nucleon. We will compare the IMF production from different decay processes inside the same nuclear events. In fact, it will be investigated the role played by phenomena involving local, dynamically driven neck instabilities coupled to QP multifragmentation. In this way a detailed comparison between the IMF produced via statistical and dynamical processes will be driven on the basis of the isotopic composition of the fragments.

In Section 2 a description of the experimental conditions is given; in Section 3 we briefly review the Classical Molecular Dynamics (CMD) model and the Statistical Multifragmentation Model (SMM), used in this paper. Section 4 is devoted to describe the impact parameter selection procedure. In Section 5 the experimental results concerning the midperipheral collisions are presented. The characterisation of IMF produced in the different processes is presented in Sections 6 and 7 and discussed in Section 8, then the conclusions are drawn in Section 9.

## 2. Experimental method

The experiment was performed at the INFN Laboratorio Nazionale del Sud with the MEDEA [10] and MULTICS [11] experimental apparatus. A beam of $^{58}$Ni at 30 MeV/nucleon bombarded a 2 mg/cm$^2$ thick nickel target. The angular range $3^\circ < \theta_{\mathrm{lab}} < 28^\circ$ was covered by the MULTICS array [11]. The MULTICS array consists of 55 telescopes, each of which was composed of an Ionization Chamber (IC), a silicon position-sensitive detector (Si) and a CsI crystal. The typical values of the energy resolutions are 2%, 1% and 5% for IC, Si and CsI, respectively. The identification thresholds in the MULTICS array were about 1.5 MeV/nucleon for charge identification. A good mass resolution for light isotopes (up to carbon) was obtained. Energy thresholds for mass identification of 8.5, 10.5, 14 MeV/nucleon were achieved for $^4$He, $^6$Li and $^{12}$C nuclei, respectively. The $4\pi$ detector MEDEA consists of a ball built up with 180 barium fluoride detectors placed at 22 cm from the target and it is able to measure and identify light charged particles ($Z = 1, 2$) ($E \leqslant 300$ MeV) and $\gamma$-rays up to $E_\gamma = 200$ MeV in the polar angles from $30^\circ$ to $170^\circ$ and in the whole azimuthal angle [10]. The charge ($Z = 1, 2$) identification thresholds in the MEDEA array were about 4 MeV/nucleon.

The geometric acceptance of the combined array was greater than 90% of $4\pi$.

In this experiments light charged particle and fragments were detected on an event by event basis, thus allowing a rather complete description of the reaction dynamics.

## 3. Brief description of models used in data analysis

### 3.1. The classical molecular dynamics model

In this model [12] it is assumed that each nucleon of the Ni nuclei moves under the influence of a two body potential $V$ consisting of two different interactions [13]: the first one, for identical nucleons, is purely repulsive so no bound state of identical nucleons can exist (to mimic in some sense the Pauli principle), and the second, for proton–neutron interaction, is attractive at large distances and repulsive at small ones. This potential gives an EoS of classical matter having about 250 MeV of compressibility. The EOS strikingly resembles that of nuclear matter (i.e., equilibrium density $\rho_0 = 0.16\ \text{fm}^{-3}$ and energy $E(\rho_0) = -16$ MeV/nucleon).

Both nuclei are initialised in their ground state by using the frictional cooling method [14], then they are boosted towards each other. Energy and momentum are conserved. In Refs. [5,13,15] it is shown that many experimental data on heavy ion collisions are reasonably explained by this classical model. However, even though this model takes into account all order correlations at the classical level, and this is quite important when studying instabilities, one has to note that the classical structure of the model leads to an explosive behaviour concerning the amount of emitted fragments and the impossibility of forming fragments at midvelocity (at the energies here considered). This last point concerns the fact that the available energy per nucleon do not classically allow to bound fragments in the neck region.

### 3.2. The statistical multifragmentation model

The statistical multifragmentation model is based on the assumption of statistical equilibrium at a low density freeze-out stage of the nuclear system formed during the collision. At this stage, primary fragments are formed according to their equilibrium partitions. Equilibrium partitions are calculated according to the microcanonical ensemble of all break-up channels composed of nucleons and excited fragments of different masses. The model conserves energy, momentum, mass and charge numbers. The statistical weight of decay channel $j$ is given by $W_i \propto \exp[S_j(E_s^*, V_s, A_s, Z_s)]$, where $S_j$ is the entropy of the system in channel $j$ and $E_s^*$, $V_s$, $A_s$ and $Z_s$ are the excitation energy, volume, mass and charge numbers of the fragmenting source. Different breakup configurations are initialised according to their statistical weights. The fragments are then propagated in their mutual Coulomb field and allowed to undergo secondary decay. Light fragments with mass number $A_f \leqslant 4$ are considered as stable particles with only translational degrees of freedom; fragments with $A_f > 4$ are treated as heated nuclear liquid drops. The secondary decay of large fragments ($A_f > 16$) is calculated from an evaporation–fission model, and that of smaller fragments from a Fermi breakup model [6,16].

## 4. Data analysis prescriptions

In heavy ions reactions at intermediate energies different decaying systems are formed depending on impact parameter. These systems behave as fragment sources which differ in size, shape, excitation energy, and even the way in which they are formed. Therefore, from the experimental point of view, one has to adopt a procedure of data analysis which allows to identify the emitting systems and assures that all the selected fragments can be assigned to one of these systems. Then, since the aim of this paper is to present data on IMF production in the following we will restrict our analysis only on multifragmentation events [17]. In this respect, we found multifragmentation production in central and midperipheral collisions ($b \leqslant 6$–$7$ fm), while most peripheral ones are characterised by quasi-elastic and elastic scattering. The impact parameter data selection is based on the heaviest fragment velocity. In fact, it appears that we can select peripheral and midperipheral events when the heaviest fragment (produced by the disassembly of a QP emitting source) travels in the laboratory frame at velocities higher than 80% of that of the projectile ($v_P = 7.6$ cm/ns); on the contrary the central collisions are labelled as those in which the heaviest fragments travels at velocities close to that of the centre of mass ($v_{cm} = 3.8$ cm/ns). We have to remember that in the analysis we consider only "complete" events, with at least 3 IMF produced, for which the heaviest fragments has a charge $Z \geqslant 9$ and at least 80% of the total linear momentum was detected. Accordingly, since the energy thresholds make not possible the detection of the QT reaction products, we find that the total detected charge ($Z_{Tot}$) does not differ from that of the projectile for more than 30% ($20 \leqslant Z_{Tot} \leqslant 36$).

In order to test the reliability of the selection criteria we compared the experimental data with the predictions of classical molecular dynamics calculations (CMD) [12], by means of the variable suggested in Ref. [18]:

$$\eta = \frac{\sum_{i=1}^{m} E_i}{\sum_{i=1}^{m} A_i},$$

where $E_i$ and $A_i$ are the energy in the centre of mass reference frame and the mass of the $i$th IMF in the event, respectively. It is expected from simulations that the quantity $\eta$ is large for peripheral collisions and small for more central ones. It should be noted that the detection thresholds affect the values of the experimental $\eta$ parameter, in particular, selecting the higher impact parameters.

In Fig. 1(a) is plotted the $\eta$ distribution as a function of the impact parameter for events generated by the CMD model; a clear increase of this observable for increasing impact parameters is evident. In Fig. 1(b) it is presented the average multiplicity of IMF, predicted by the CMD model, as a function of the impact parameter. One can see how multifragmentation appears for midperipheral and central collisions; moreover, it is not surprising the fact that the maximum of $\langle N_{IMF} \rangle$ is around $b = 4$ fm (exactly at midperipheral collisions) because we are in the situation for which still two separate systems (the QP and the QT) can survive with a maximum in their excitation energy.

Focusing our attention on midperipheral collisions we show in Fig. 1(c) the $\eta$ distribution predicted by the CMD model for impact parameters in the range $3 \leqslant b \leqslant 6$ fm (full set of

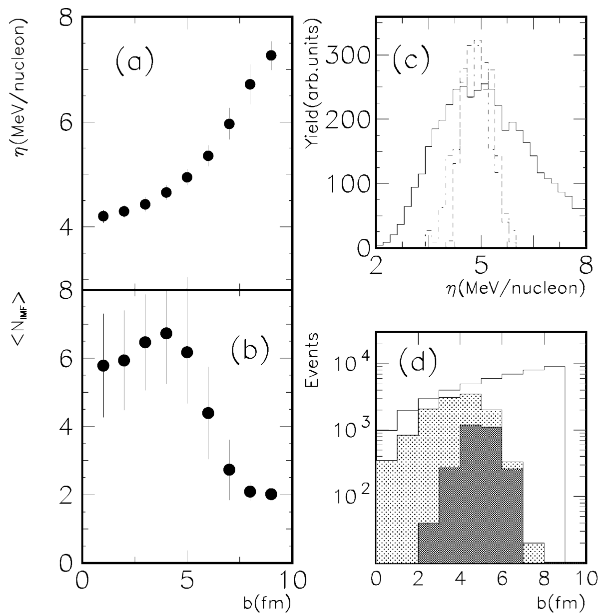


Fig. 1. (a), (b) $\eta$ distribution and average multiplicity of IMF predicted by CMD as a function of the impact parameter $b$; (c) $\eta$ distribution predicted by CMD for impact parameters in the range $3 \leqslant b \leqslant 6$ fm (dashed line: full set of data, dot-dashed line: after experimental efficiency filtering) and experimental $\eta$ distribution (full line) for events that fulfil the prescription of midperipheral collisions data selection (see text); (d) Yields from CMD calculations: raw data (blank area), multifragmentation events after apparatus efficiency (dot-filled area), with further constraints on the heaviest fragments (dark area).

data and after the experimental efficiency filtering has been taken into account) and the amount of "complete" experimental multifragmentation events that fulfil the prescription of midperipheral collisions data selection (see above). We find encouraging signals of a good data selection (the maximum of $\eta$ catches the same value), even if the experimental distribution, due to the experimental efficiencies and resolutions, is much broader than the predicted one. In the following we will show that this broadening depends also on the appearance of dynamical IMF production, not present in the CMD predictions.

How midperipheral impact parameter are preferentially selected becomes evident also from Fig. 1(d): the dot-filled area refers to the amount of "complete" multifragmentation events (with at least three IMF products) after experimental efficiency filtering. In the dark area of Fig. 1(d) we present the filtered complete events with the further condition that the heaviest fragment moves with a velocity higher than the 80% of $v_P$.

## 5. The midperipheral collisions

Being confident on the data selection the results presented in the following will focus only on midperipheral collisions, with the aim of study the IMF production. In Fig. 2

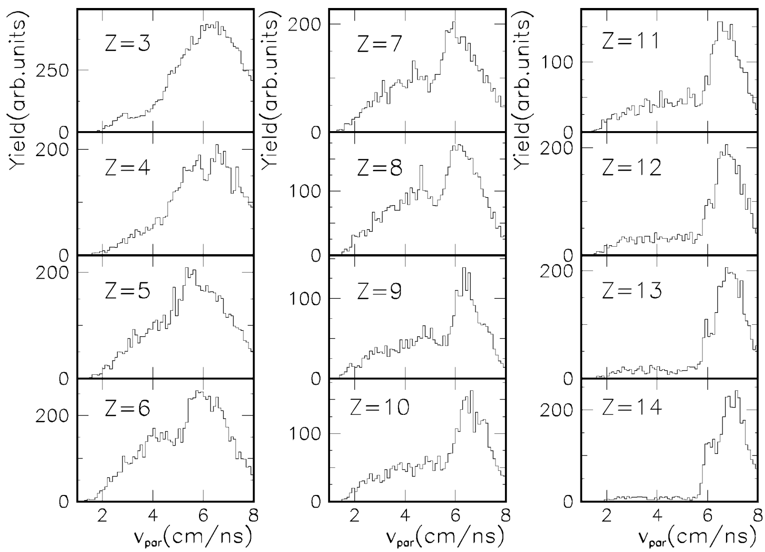


Fig. 2. Experimental $v_{\mathrm{par}}$ distributions for $Z = 3$–14.

the yields of different fragments in the range $3 \leqslant Z \leqslant 14$ are plotted as a function of the parallel component of the velocity, with respect to the beam axis. In the distributions two distinct region can be observed for $6 \leqslant Z \leqslant 9$, corresponding to an emission from a QP fast moving (with velocity around 6.5 cm/ns) and an IMF production at midvelocity (3.8 cm/ns, around the centre of mass velocity, due to the system symmetry).

In order to better investigate the midvelocity component we compared the experimental results with the prediction of the CMD model. In Fig. 3 the velocity distributions for midperipheral impact parameter ($3 \leqslant b \leqslant 6$ fm) are shown; we find an overlap at midvelocity between the QP and QT contributions only for the lighter nuclei ($Z \leqslant 4$). The CMD model do not predict any occurrence of non-statistical structures at midvelocity, due to its “classical” nature; in this framework only light particles are emitted between the two sources. On the contrary one has to note that, if only two emitting sources are present the velocity distributions of fragments with charge $Z \geqslant 5$ are well separate in the velocity space.

We then decided to study what one has to expect from pure statistical decay of a QP and a QT excited sources. In this respect we based on the Statistical Multifragmentation Model (SMM) [16], which succeeds in the explanation of many experimental results [19,20]. The calculations were performed for a Ni nucleus at one third of the normal density. The events were generated by SMM for an excitation energy of 4 MeV/nucleon for both sources; this choice comes from the indications obtained in a previous study [17]. In Ref. [21] it has been shown that a mutual Coulomb influence can occur in presence of large emitting sources (Au-like); the effect is a distortion in the parallel velocity distributions, that tends to fill the velocity region intermediate between the two sources. In the present case the emitting sources are relatively small and this effect does not take an important role in the velocity distributions. In Fig. 4 the SMM predictions concerning the parallel component of

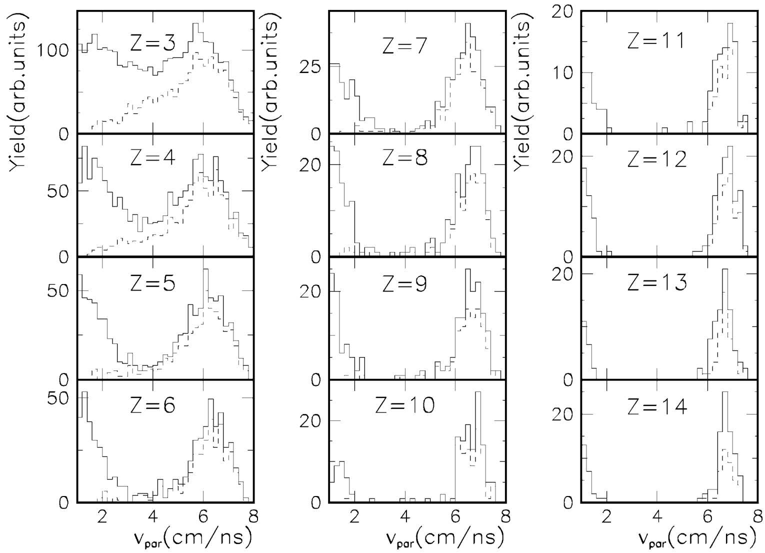


Fig. 3. CMD predictions for $v_{\rm par}$ distributions for $Z = 3$–14 (full set of data: full line, after efficiency filtering: dashed line).

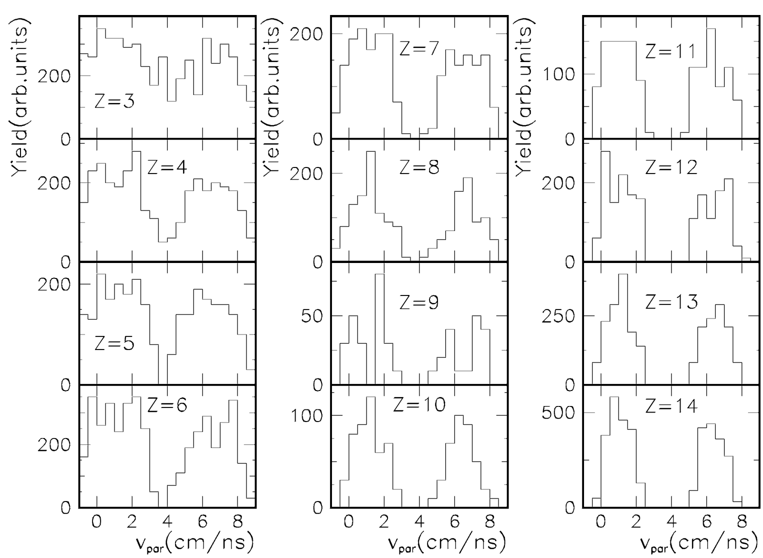


Fig. 4. SMM predictions for $v_{\rm par}$ distributions for $Z = 3$–14.

the velocity are shown for $3 \leqslant Z \leqslant 14$. Once more one can observe that an overlap between the QP and the QT velocity distribution takes place only for light fragments ($Z \leqslant 4$).

As a further check we made a test using directly the experimental data. In the following section indications of a statistical decay of a thermalized QP emitting source will be shown. Then, basing on the hypothesis that all the fragments moving at velocities higher than 6.5 cm/ns are emitted from the QP we can simulate the clean distributions of the QP

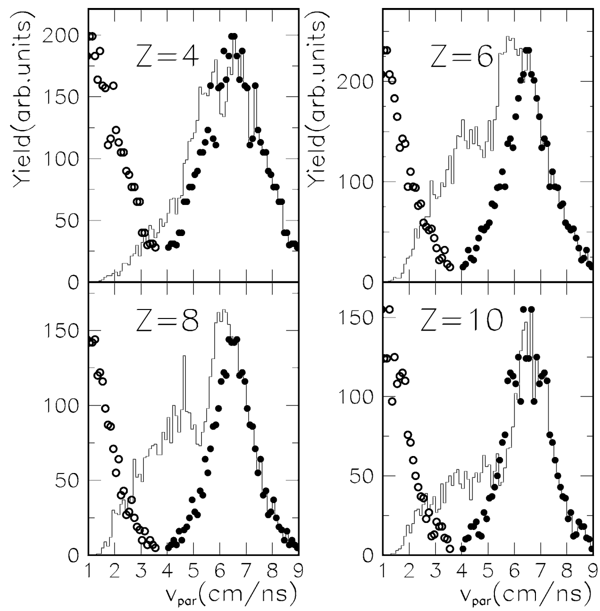


Fig. 5. Simulated $v_{\text{par}}$ distributions for $Z = 4$, 6, 8, 10, originating from QP (full points) and QT (open points); the experimental yield for velocities higher than 6.5 cm/ns has been used to generate the slower part of the QP and the QT contributions.

and of the QT, by backward reflecting the experimental QP distributions and conserving the linear momentum. In Fig. 5 are shown the obtained results (for $Z = 4$, 6, 8, 10); it is evident that the midvelocity component can not completely be ascribed to an emission from the statistical decay of the QP and of the QT.

Concerning the above discussion on the velocity distributions we can summarise claiming that different IMF sources are contemporarily present in the same physical event: the QP and QT (which fragments are not experimentally seen because under energy threshold for identification) sources and a midvelocity emission source, that can be described as a neck formed during the overlap of projectile and target.

## 6. The QP emitting source

In order to study the process leading to the disassembly of the QP we restrict the analysis to the fragments emitted with $v_{\text{par}} > 6.5$ cm/ns. This constraint allows the selection of the decay products forward emitted in the QP decay with negligible contamination due to QT and midvelocity source emission. To check if the QP reaches an equilibration stage before its de-excitation we studied in its reference frame the angular and energy distribution of the emitted isotopes.

One has to remember that the energy distributions can be strongly influenced by the fact that Coulomb and collective energies are mass dependent; in this case energy spectra of different isotopes may display different slopes. On the contrary, the thermal

Table 1
Temperature parameters extracted from a maxwellian fit procedure of the isotope energy spectra (typical fit error on extracted values is ±1 MeV)

| $Z$ | $A$ | $T_{\mathrm{slope}}$ (MeV) | $Z$ | $A$ | $T_{\mathrm{slope}}$ (MeV) |
|---|---|---|---|---|---|
| 3 | 6 | 7.8 | 5 | 10 | 9.6 |
| 3 | 7 | 9.0 | 5 | 11 | 10.0 |
| 3 | 8 | 7.8 | 5 | 12 | 10.0 |
| 4 | 7 | 9.7 | 6 | 12 | 8.7 |
| 4 | 9 | 10.5 | 6 | 13 | 9.1 |
| 4 | 10 | 9.7 | | | |

energy contribution has to be the same for all masses. By fitting energy distributions with a Maxwellian function (for a surface emission)

$$Y(E) = \frac{(E - E_0)}{T_{\mathrm{slope}}^2} e^{\frac{-(E-E_0)}{T_{\mathrm{slope}}}}, \tag{1}$$

where $E_0$ is a parameter related to the Coulomb repulsion, we get similar values (within errors) for all the detected isotopes ($3 \leqslant A \leqslant 14$) for the parameter related to the apparent temperatures $T_{\mathrm{slope}}$. The fit results are presented in Table 1. It is possible to note the similarity of the slopes, independent from the considered isotope. As an example in Fig. 6 the energy distribution of different lithium isotopes are presented; the results of the maxwellian fit are superimposed.

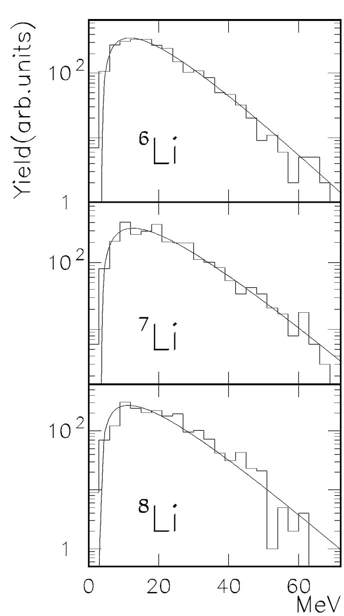


Fig. 6. Energy distributions for different isotopes of the lithium; maxwellian fit are superimposed.

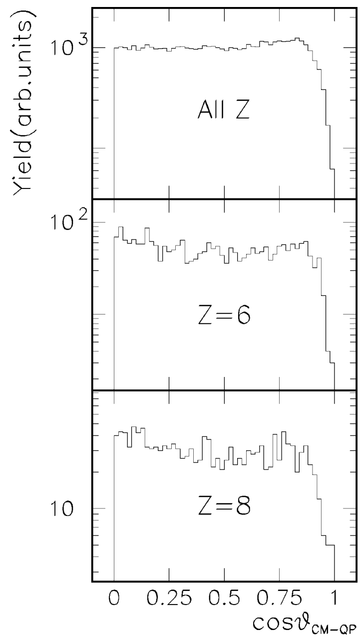


Fig. 7. Angular distributions for IMF forward emitted by the QP.

This behaviour gives indications that the condition of equilibration of the fragmenting systems is satisfied.

The aim of the investigation of the angular distributions is to verify if the fragments were emitted from a nearly isotropic source as expected for a statistical decay.

Angular distributions are presented in Fig. 7; they present a flat behaviour, in agreement with the hypothesis of an isotropic emission; this is also a necessary condition to establish a possible equilibration of the studied system.

Since energy and angular distributions satisfy some necessary condition that support the hypothesis that the QP has been subject to an equilibration process we can compare its experimental distributions with the predictions of a statistical multifragmentation model. SMM well described the experimental findings of fragment emission in the present expected excitation energy regime [19]. The calculation were performed for a Ni nucleus at one third of the normal density. The events generated by SMM for different input excitation energies were filtered by the apparatus. The experimental charge distribution is properly reproduced by choosing an excitation energy of 4 MeV/nucleon for the decaying source (Fig. 8).

As a section summary we want to stress that the QP decay shows indications that equilibrium has take place and then, that the de-excitation can be described in statistical terms.

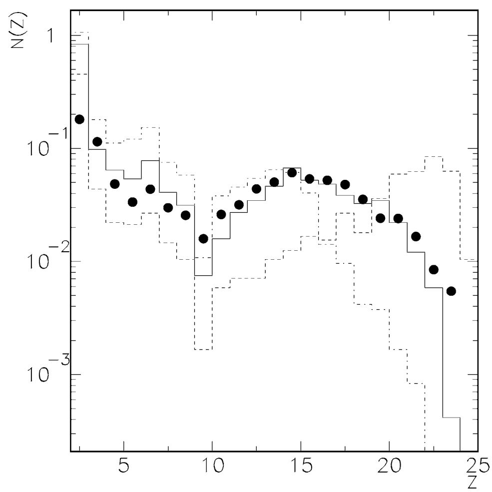


Fig. 8. Mean elemental event multiplicity $N(Z)$ for QP fragments (solid point: experimental data, histogram: SMM predictions (dashed line: $E^* = 3$ MeV/nucleon, full line: $E^* = 4$ MeV/nucleon, dot-dashed line: $E^* = 5$ MeV/nucleon)).

## 7. Evaluation of neck IMF characteristics

As clearly shown in Fig. 2 a large amount of IMF (mainly for $Z = 6$–$10$ values) are emitted at midvelocity. These fragment could be produced in multifragmentation processes, but their presence at intermediate velocities, contemporarily to fragments coming from a QP disassembly, can not be explained in terms of statistical theory. In this section we will present evidences that the IMF emitted at midvelocity are of a different origin.

Since the characteristics of the QP are already well established, in this section we will investigate the charge and isotopic distributions of the IMF emitted at midvelocity by means of fit procedures, described in the following.

The starting point consists in the evidence that the fragments emitted with velocities higher than that of the QP (forward emission from the QP) only come from the QP (i.e., for $v_{\mathrm{QP}} \geqslant 6.5$ cm/ns the distributions are not contaminated by IMF coming from the midvelocity region). In fact, the only possible contamination of velocity distributions could appear by mixing central and peripheral collisions: a strong coulomb burst is necessary to push fragments in the QP velocity region and only a large emitting source (e.g., the compound nucleus formed in the central collisions) can succeed. As an example a $Z = 3$ fragment, emitted by a compound nucleus formed in the most central collisions, due to the coulomb repulsion by the emitter, can reach (in the laboratory frame) velocities not higher than 6.0 cm/ns. The data selections prevent this kind of central-peripheral mixing and then we are confident that the forward emitted QP distributions are clean from contaminations coming from different sources (see also the angular and energy distributions presented in the previous section).

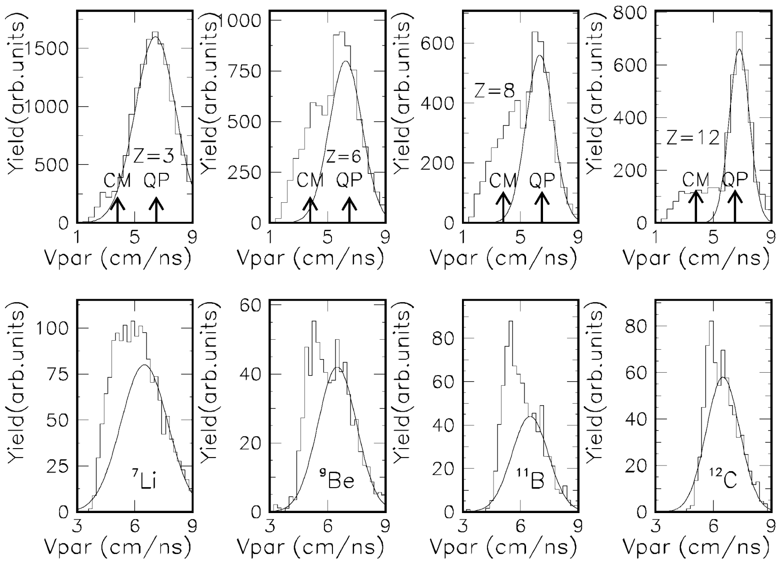


Fig. 9. Experimental $v_{par}$ distributions and superimposed fit for the QP contribution; the arrows refer to the centre of mass (CM) and QP velocities.

Then, the first step consists in the definition of the velocity distributions of the fragments coming from the disassembly of the QP. We took into account only the forward emission region and fitted the velocity distributions by means of gaussian functions, with the maximum fixed at the QP velocity. This fit was performed for each charge in the range $Z = 3$–14 (giving the QP yield $Y_{QP}(Z)$ and for each isotope for the Li, Be, B and C cases, $Y_{QP}(Z, A)$). The fit results are presented in Fig. 9.

Due to the experimental energy threshold (for the QT source side) the velocity spectra are not symmetric around the c.m. velocity. To avoid possible contamination in the midvelocity region we evaluated the yield ($Y_{NECK}$) at midvelocity as twice the difference between the whole $v_{par}$ distribution for velocities higher than that of the c.m. and $Y_{QP}$. This was done to avoid distortions due to efficiency effects and possible QT contaminations for the lowest velocities. We checked that in the considered $Z$ range the experimental inefficiencies do not affect the above-mentioned procedure [11].

Starting from the values extracted from the fits we can compare the characteristics of the neck IMF properties versus the QP ones. As shown in Fig. 10, the charge distributions of the two IMF contributions (QP and midvelocity) are very different. In particular there is a higher probability of production from the neck of IMF with charge between that of the carbon and of the oxygen.

In addition, in Fig. 11 are presented the parallel to the beam component of the velocity for several fragments. From these plot it appears that the neutron-rich isotopes are mainly emitted at midvelocity. In Fig. 12 the ratio between the yields of the heavier and the lighter isotope of each $Z$ are plotted as a function of the parallel component of the velocity. One can see as this ratio decreases going towards the higher velocities (QP region). This

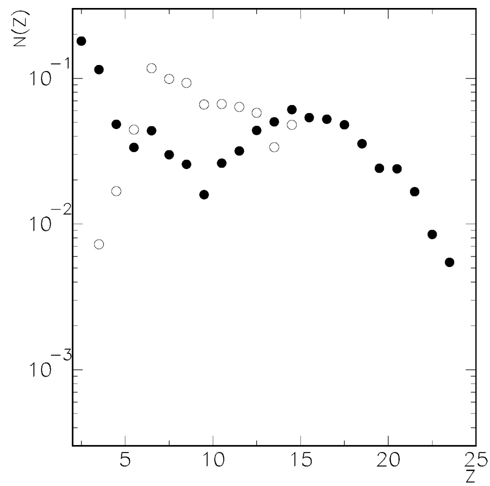


Fig. 10. Mean elemental event multiplicity $N(Z)$ for QP fragments (solid point) and midvelocity region fragments (open points).

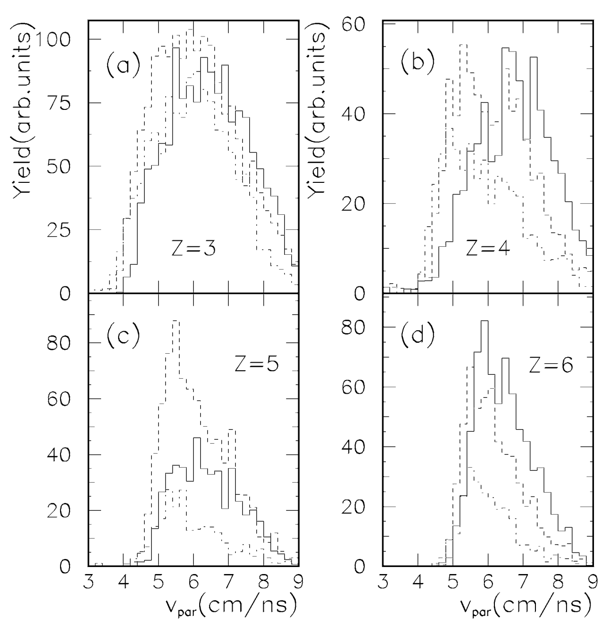


Fig. 11. Experimental $v_{par}$ distributions for different isotopes (full line: $^{6}$Li, $^{7}$Be, $^{10}$B, $^{12}$C; dashed line: $^{7}$Li, $^{9}$Be, $^{11}$B, $^{13}$C; dot-dashed line: $^{8}$Li, $^{10}$Be, $^{12}$B, $^{14}$C).

behaviour suggests that the IMF coming from a neck-like structure differ from those coming from the QP disassembly even for what concern the isotopic composition.

In order to verify if this behaviour could be due to a mere kinematical reason we made a comparison with the filtered prediction of the CMD model. As already discussed in these predictions no midvelocity component is present. In Fig. 13 the ratios between the yields

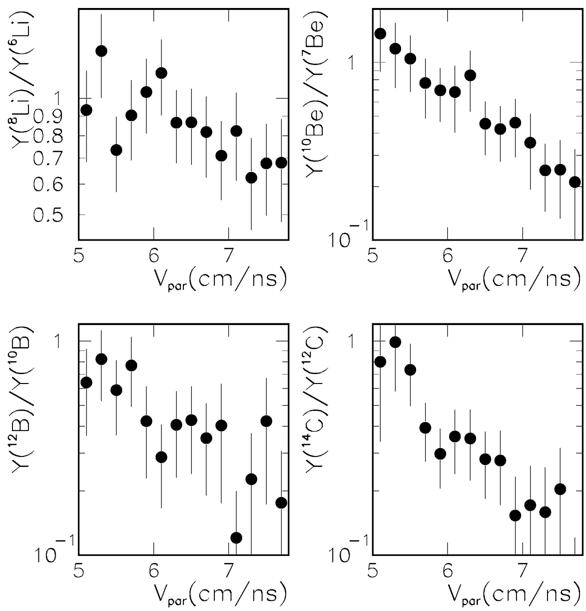


Fig. 12. Experimental yield ratios (heavy isotope/light isotope) as a function of $v_{\mathrm{par}}$.

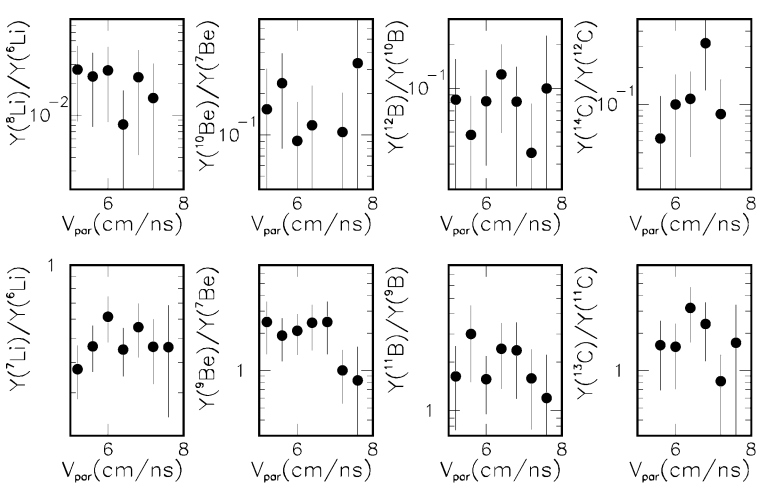


Fig. 13. CMD predictions for yield ratios (heavy isotope/light isotope) as a function of $v_{\mathrm{par}}$.

of the heavier and the lighter isotope of each $Z$ as a function of the parallel component of the velocity are presented. In this case, since all fragments are coming from the QP, we get a flat trend for this ratio.

From the fit procedure it is also possible to extract quantitative values for the isospin composition of the neck IMF. However, in this case we have to introduce other constraints to the analysis method. In fact, the energy thresholds to extract the mass value of the detected fragments are much higher than that allowing the charge discrimination (see

Section 2 for details). Then, when looking at velocity distributions, if on one side the energy thresholds do not affect the QP and neck amounts for fixed $Z$ values (concerning $v \geqslant 3.8$ cm/ns), on the contrary the mass restrictions are present in the neck part, when single isotopes are concerned. As starting point we have:

$$Y(Z) = Y_{\mathrm{QP}}(Z) + Y_{\mathrm{NECK}}(Z), \tag{2}$$

$$\sum Y_{\mathrm{QP}}(Z, A_i) = K(Z) Y_{\mathrm{QP}}(Z), \tag{3}$$

$$\sum Y_{\mathrm{NECK}}(Z, A_i) = K(Z) Y_{\mathrm{NECK}}(Z), \tag{4}$$

where $Y(Z)$ is the total yield at fixed $Z$ values and $Y(Z, A_i)$ is the yield of the isotope $(Z, A_i)$; in Eqs. (3), (4) the sum run on all the $i$ isotopes of the $Z$ fixed atomic species and the factor $K(Z)$ has been introduced to take into account the fact that few detectors do not present a sufficient resolution to distinguish the mass numbers and were not considered in the extraction of the $Y(Z, A_i)$ values. Moreover, looking at single isotope distributions, we define

$$Y_{\mathrm{NECK}}^{\mathrm{exp}}(Z, A) = Y_{\mathrm{exp}}(Z, A) - Y_{\mathrm{QP}}(Z, A),$$

where $Y_{\mathrm{exp}}(Z, A)$ corresponds to the whole experimental yield (note that no cuts affect the QP component, $Y_{\mathrm{QP}}^{\mathrm{exp}}(Z, A) = Y_{\mathrm{QP}}(Z, A)$).

The relation between the $Y_{\mathrm{NECK}}^{\mathrm{exp}}(Z, A)$ measured yield (affected by the detection efficiency) and the "true" yield $Y_{\mathrm{NECK}}(Z, A)$ can be recovered in the form:

$$Y_{\mathrm{NECK}}^{\mathrm{exp}}(Z, A) = \varepsilon_{\mathrm{NECK}}(Z, A) Y_{\mathrm{NECK}}(Z, A), \tag{5}$$

where $\varepsilon_{\mathrm{NECK}}(Z, A)$ represents the experimental efficiency to that given isotope.

Then from Eq. (4) we must have:

$$\begin{aligned} K(Z) Y_{\mathrm{NECK}}(Z) &= \sum Y_{\mathrm{NECK}}(Z, A_i) = \sum \frac{Y_{\mathrm{NECK}}^{\mathrm{exp}}(Z, A_i)}{\varepsilon_{\mathrm{NECK}}(Z, A_i)} \\ &= \sum \frac{(Y_{\mathrm{exp}}(Z, A_i) - Y_{\mathrm{QP}}(Z, A_i))}{\varepsilon_{\mathrm{NECK}}(Z, A_i)}. \end{aligned} \tag{6}$$

At this point we have to introduce the hypothesis that the experimental efficiency $\varepsilon_{\mathrm{NECK}}(Z, A)$ is weakly dependent on the mass number ($\varepsilon_{\mathrm{NECK}}(Z, A) \simeq \varepsilon_{\mathrm{NECK}}(Z)$); this approximation do not play a significant role if we consider only $Z \geqslant 3$ values since the velocity threshold do not vary significantly from one isotope to another of the same atomic species (see, for instance, at Fig. 11).

Then, from Eq. (6) we have:

$$\varepsilon_{\mathrm{NECK}}(Z) K(Z) = \frac{\sum (Y_{\mathrm{exp}}(Z, A_i) - Y_{\mathrm{QP}}(Z, A_i))}{Y_{\mathrm{NECK}}(Z)}.$$

The factor $K(Z)$ can be extracted from Eq. (3) and then, once calculated $\varepsilon_{\mathrm{NECK}}(Z)$, we can extract the "true" $Y_{\mathrm{NECK}}(Z, A)$ contribution.

The obtained results for the neck IMF together with the QP measured values are plotted in Fig. 14; it is clear that the IMF coming from the neck are neutron rich, when at the contrary the QP contribution is mainly based on lighter isotopes. To better present this

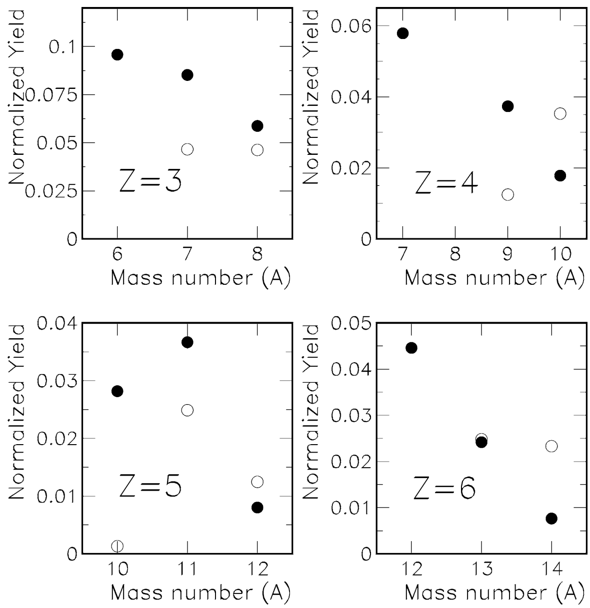


Fig. 14. Isotope yields for different fragments normalized to the number of events (full symbols: QP fragments, open symbols: neck fragments).

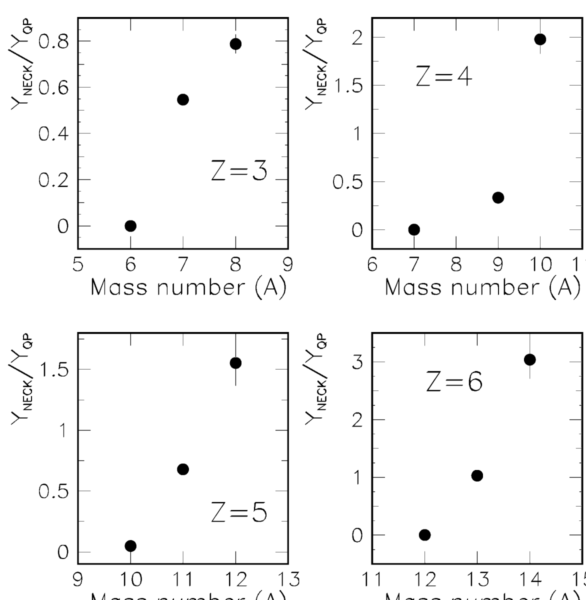


Fig. 15. Yield ratios between the contributions of the midvelocity region and of the QP as a function of the mass number.

fact in Fig. 15 the ratio between the two contributions as a function of the mass number is presented. In these last two figures only statistical errors are considered; in any case the presence of systematic errors in the approximation can not affect the observed trends. Moreover, looking at the average values of the $N/Z$ ratio for different $Z$ numbers (results presented in Table 3), it appears that, if from one side the QP products have values still close to that of the starting system (1.07) and very similar to those of the stable nuclei, on the other side the midvelocity fragments show a large abundance concerning the neutron content.

## 8. Discussion

In the previous sections we have shown that IMF production in midperipheral collisions is due to two different processes: the statistical decay of the QP and a dynamical emission at midvelocity.

Concerning the QP disassembly, pointed out that equilibrium of the emitting source has take place, it is full of meaning to investigate some of its thermodynamic characteristics (as the temperature and excitation energy).

We extract the temperature through double ratios of isotope yields method [22]. The double ratio $R$ of the yields $Y$ of four isotopes in their ground states, prior to secondary decay is given by:

$$R = \frac{Y(A_1, Z_1)/Y(A_1+1, Z_1)}{Y(A_2, Z_2)/Y(A_2+1, Z_2)} = \frac{e^{B/T}}{a}, \tag{7}$$

where $a$ is a constant related to spin and mass values, and

$$B = BE(Z_1, A_1) - BE(Z_1, A_1+1) - BE(Z_2, A_2) + BE(Z_2, A_2+1),$$

and $BE(Z, A)$ is the binding energy of a nucleus with charge $Z$ and mass $A$ [22]. In principle, the temperature-dependence of the isotope ratio $R$ allows for determination of the temperature $T$. However, primary fragments can be highly excited [23] so that secondary decays from higher lying states of the same and heavier nuclei can lead to non-negligible distortions of the measured ratios $R$, which need to be corrected [24] to recover information on the temperature at the freeze-out stage. To reduce the sensitivity to such corrections, it is advisable to choose cases for which $B \gg T$ since the uncertainties on $T$ are proportional to $T/B$.

Moreover, to apply the double ratios method [22] one has to be sure that the nuclei originate from the same emitting source and therefore, when the contributions of different sources are present, particular care must be taken in selecting the isotopes. Looking at $v_{\mathrm{par}}$ experimental distributions we observe a large overlap for light particles ($Z = 1$, 2), we then select only heavier fragments forward emitted ($v_{\mathrm{F}} \geqslant 6.5$ cm/ns, velocity of the QP in the laboratory frame). Table 2 presents the temperature values for thermometers with large $B$ values, that though less sensitive to secondary decay distortions, still show fluctuations due to these decays (look at the experimental $T_{\mathrm{exp}}$ values). In Refs. [24,25] an empirical procedure was proposed, to strongly reduce these fluctuations. It was also

Table 2
Temperatures extracted from different double yield isotope ratio ($T_{\mathrm{exp}}$) and calculated values after sequential feeding correction ($T_{\mathrm{corr}}$)

| | $T_{\mathrm{exp}}$ (MeV) | $T_{\mathrm{corr}}$ (MeV) |
|---|---|---|
| $^{6}$Li/$^{7}$Li – $^{11}$C/$^{12}$C | $3.9 \pm 0.2$ | $3.3 \pm 0.3$ |
| $^{9}$Be/$^{10}$Be – $^{11}$C/$^{12}$C | $6.7 \pm 0.9$ | $3.7 \pm 0.5$ |
| $^{10}$B/$^{11}$B – $^{11}$B/$^{12}$B | $4.3 \pm 0.5$ | $4.3 \pm 0.5$ |
| $^{11}$B/$^{12}$B – $^{11}$C/$^{12}$C | $4.3 \pm 0.3$ | $4.4 \pm 0.3$ |
| $^{11}$C/$^{12}$C – $^{12}$C/$^{13}$C | $3.7 \pm 0.2$ | $3.6 \pm 0.2$ |

Table 3
Average $N/Z$ ratio values

| $Z$ | $\langle N/Z\rangle_{\mathrm{QP}}$ | $\langle N/Z\rangle_{\mathrm{NECK}}$ |
|---|---|---|
| 3 | 1.28 | 1.50 |
| 4 | 1.03 | 1.43 |
| 5 | 1.14 | 1.26 |
| 6 | 1.09 | 1.25 |

shown [24] that for temperatures in the neighbourhood of 4 MeV these empirical correction factors do not depend either on the size or on the $N/Z$ ratio of the decaying systems. The experimental temperatures of the present measurement ($T_{\mathrm{corr}}$), corrected as suggested in Ref. [24] are also reported in Table 2. Averaging these values a break-up temperature $T$ of the QP decaying system of 3.9 MeV is obtained.

The obtained values for the parameter related to the apparent temperature $T_{\mathrm{slope}}$ (see Table 1) are higher than those extracted from isotope ratios. This is a well known trend, in fact several experimental studies showed that the temperature values obtained from maxwellian fits are higher than those extracted from isotope ratios or level population ratios [26]; moreover, the $T_{\mathrm{slope}}$ values are even higher than typical temperatures used in statistical models to reproduce the experimental distributions [16]. A tentative explanation of this difference has been done in the framework of standard statistical models [27]. In particular one has to take into account the Fermi-motion of nucleons [28] and variations in the Coulomb barrier depending on the point of emission within the system; one has also to remind that the $T_{\mathrm{slope}}$ values are averaged over the de-excitation chain and are also affected by successive recoil effects. In this respect, the corrected values of the temperatures extracted from isotope ratios are considered more realistic, i.e., more representative of the freeze-out temperature.

In the assumption of a statistical decay for the QP it is very interesting to investigate the coordinates of this system on the caloric curve (temperature vs. excitation energy).

For this experiment it is not possible to perform a careful evaluation of the excitation energy through calorimetry [29] since this technique requires an event by event assignment of each fragment to its emitting source, and this is not possible in the present case (due to the overlap of distributions between midvelocity and QP velocity).

Excitation energies were estimated in three different ways.

(i) By means of the calorimetric technique [29] taking into account only the heaviest fragment and the forward emitted ones (we double them in order to mimic the backward emission [30]). Large uncertainties are present in this calculation and the obtained value can give only a very raw value for the excitation energy: the average of the excitation energy turns out to be $\langle E^*/\text{nucleon}\rangle \approx 4 \pm 3$ MeV/nucleon.

(ii) Giving a rough estimation of the upper limit of the excitation energy using energy conservation and assuming that on average there is an equal sharing of excitation energy between QP and QT. Then in the centre of mass frame we have: $E^*_{\text{QP}} = \frac{1}{2}(m_\text{P} v_\text{P}^2 - m_{\text{QP}} v_{\text{QP}}^2) + E^*_{\text{NECK}}$ where $m_\text{P}$, $m_{\text{QP}}$, $v_\text{P}$, $v_{\text{QP}}$ are mass and velocity of projectile and QP, respectively. Fixing $v_\text{P} = 3.8$ cm/ns and $v_{\text{QP}} = 2.7$ cm/ns (6.5 cm/ns in the laboratory frame) and neglecting the energy transferred to the neck source we have a maximum of excitation energy of the QP depending on the amount of mass left in the centre of mass. Then we have excitation energy values increasing from 3.7 (no nucleon transfer to a neck) to 5.9 MeV/nucleon (half nickel is lost in the reaction). This rough estimation completely neglect other dissipation processes, as pre-equilibrium emission. If, for instance, we require the formation of an oxygen nucleus in the centre of mass we have accordingly an estimation of $\simeq 4.5$ MeV/nucleon.

(iii) By comparing the data with the SMM predictions [16] which well describe the experimental findings of the QP fragment emission (Fig. 8). In this case the best agreement between experimental data and predictions is found fixing at 4 MeV/nucleon the value of the excitation energy of the emitting source.

All these methods indicate that the excitation energy of the QP system is around 4 MeV/nucleon.

One can compare these values with that obtained in the study of the symmetric reaction $^{197}\text{Au} + ^{197}\text{Au}$ at 35 MeV/nucleon, for which excitation energy and temperature have been directly experimentally measured [20]; even in this case, and then in full agreement with the present experiment, to a temperature of $3.9 \pm 0.2$ MeV corresponds a measured values of $\simeq 4$ MeV/nucleon (and an upper limit of the excitation energy $\simeq 4.5$ MeV/nucleon).

We can then summarise that the QP has got thermal characteristics ($E^* \simeq 4$ MeV, $T \simeq 3.9$ MeV) for which multifragmentation takes place as the main de-excitation process.

If on one side the QP disassembly is ruled by statistical models after thermal equilibrium has been reached, on the other side the midvelocity emission exhibit quite different features that cannot be reproduced making statistical equilibrium assumptions. In particular it has been shown that significant differences appear concerning charge distribution and isotopic composition of the emitted fragments. The most striking characteristic is that the fragments coming from the midvelocity region are more neutron rich than those from the QP and the average values of the $N/Z$ ratio are much larger than the $N/Z$ of the initial system. This feature can not be explained in terms of statistical approaches and can be understood only following the dynamics of the reaction.

We have thus performed BNV calculations using different EoS parameters [9]. We found that with a compressibility term $K$ of 200 MeV (soft EoS) there is an evident massive neck formation (after 200 fm$/c$), that is not reabsorbed by the QP or the QT (this behaviour disappears increasing the $K$ values). These calculations predict that on average we have a $Z = 8$ fragment at midvelocity, and show that the IS fragment production comes from material which is "surface-like" (since it originates from the overlap of the surfaces of the two nuclei) and which could be neutron rich.

## 9. Conclusions

In the study of the $^{58}$Ni + $^{58}$Ni 30 MeV/nucleon dissipative midperipheral collisions it has been possible to investigate the characteristics of IMF produced by two different types of reaction mechanisms. The data analysis prescriptions for the impact parameter selection allowed to select a well defined set of events; in particular it has been possible to select events in which the IMFs are competitively emitted by the decay of the QP (and the QT) and by an intermediate velocity source.

Concerning the disassembly of the QP it has been verified that the system reaches a thermal equilibrium before decaying following a statistical pattern. This point was clarified looking at the experimental angular and energy distributions; isotropic angular distributions and maxwellian shape for the energy distributions give an indication that the thermalization has taken place. A comparison with the SMM predictions strongly supports this hypothesis. The temperature of the QP have been evaluated with the technique of the double ratios of isotope yields. The temperature and excitation energy values ($T = 3.9 \pm 0.2$ MeV, $E^* \simeq 4$ MeV/nucleon) locate the system in a region of the phase diagram where the multifragmentation is the main de-excitation channel.

IMF productions is present also at midvelocity, due to dynamical processes that involve the overlap of projectile and target during the collision. We have to stress that these IMFs show a very different behaviour for what concern the charge distribution and the isotopic content of the fragments. These features can be considered as a signature of a non statistical origin of these IMFs. Moreover, statistical models do not predict charge distributions as that observed for midvelocity fragments.

By comparing experimental IMF characteristics, it appears that those coming from dynamical processes are more neutron rich than the average matter of the overall system, even though the $N/Z$ ratio of the whole system is closed to the unity. In fact, while in the case of the QP fragments the average values of the $N/Z$ ratio for each element are similar to those of stable nuclear matter, the neck products present a large neutron content. A neck formation in the present reaction can be accounted by soft EoS. BNV calculations with a compressibility term of 200 MeV predict that the neck comes from surface interactions of the nuclei and, therefore, the neutron content is higher.

## Acknowledgements

The authors are gratefully to M. Belkacem, A. Bonasera and A.S. Botvina for the avalaibility of their codes. The authors are also indebted to R. Bassini, C. Boiano, S. Brambilla, G. Busacchi, A. Cortesi and M. Malatesta for their skillful assistance.

## References

[1] U. Mosel et al., Nucl. Phys. A 236 (1974) 252;
G. Sauer et al., Nucl. Phys. A 264 (1976) 221;
H.R. Jaqaman et al., Phys. Rev. C 27 (1983) 2782;
H.R. Jaqaman et al., Phys. Rev. C 29 (1984) 2067.
[2] J. Pochodzalla et al., Phys. Rev. Lett. 75 (1995) 1040.
[3] J.B. Elliot et al., Phys. Rev. C 49 (1994) 3185;
M.L. Gilkes et al., Phys. Rev. Lett. 73 (1994) 1590.
[4] J.A. Hauger et al., Phys. Rev. Lett. 77 (1996) 235;
J.A. Hauger et al., Phys. Rev. C 57 (1998) 764.
[5] P.F. Mastinu et al., Phys. Rev. Lett. 76 (1996) 2646;
A. Bonasera, M. Bruno, C.O. Dorso, P.F. Mastinu, Riv. Nuovo Cimento 23 (2000) 1.
[6] J.P. Bondorf et al., Nucl. Phys. A 444 (1986) 460.
[7] M. D'Agostino et al., Phys. Lett. B 473 (2000) 219.
[8] G. Casini et al., Phys. Rev. Lett. 71 (1993) 2567;
C.P. Montoya et al., Phys. Rev. Lett. 73 (1994) 3070;
L.G. Sobotka et al., Phys. Rev. C 50 (1994) R1272;
J. Toke et al., Phys. Rev. Lett. 75 (1995) 2920;
J.F. Dempsey et al., Phys. Rev. C 54 (1996) 1710;
Y. Larochelle et al., Phys. Rev. C 55 (1997) 1869;
J. Lukasik et al., Phys. Rev. C 55 (1997) 1906;
P. Pawlowski et al., Phys. Rev. C 57 (1998) 1711;
E. Plagnol et al., Phys. Rev. C 61 (1999) 014606;
R. Wada et al., Phys. Rev. C 62 (2000) 034601;
M. Veselsky et al., Phys. Rev. C 62 (2000) 041605(R);
Y. Larochelle et al., Phys. Rev. C 62 (2000) 051602(R).
[9] W. Bauer et al., Phys. Rev. Lett. 69 (1992) 1888;
M. Colonna et al., Nucl. Phys. A 583 (1995) 525;
M. Colonna et al., Nucl. Phys. A 589 (1995) 2671.
[10] E. Migneco et al., Nucl. Instrum. Methods Phys. Res. A 314 (1992) 31.
[11] I. Iori et al., Nucl. Instrum. Methods Phys. Res. A 325 (1993) 458.
[12] M. Belkacem et al., Phys. Rev. C 52 (1995) 271.
[13] R.J. Lenk, T.J. Schlagel, V.R. Pandharipande, Phys. Rev. C 42 (1990) 372.
[14] L. Wilet et al., Nucl. Phys. A 282 (1977) 341.
[15] V. Latora, A. Del Zoppo, A. Bonasera, Nucl. Phys. A 572 (1994) 477.
[16] A.S. Botvina et al., Nucl. Phys. A 475 (1987) 663;
J.P. Bondorf et al., Phys. Rep. 257 (1995) 133.
[17] P.M. Milazzo et al., Phys. Lett. B 509 (2001) 204.
[18] P. Pawlowski et al., Z. Phys. A 357 (1997) 387.
[19] M. D'Agostino et al., Phys. Lett. B 371 (1996) 175;
P.M. Milazzo et al., Phys. Rev. C 60 (1999) 044606.
[20] P.M. Milazzo et al., Phys. Rev. C 58 (1998) 953.

[21] A.S. Botvina, M. Bruno, M. D'Agostino, D.H.E. Gross, Phys. Rev. C 59 (1999) 3444.
[22] S. Albergo et al., Nuovo Cimento 89 (1985) 1.
[23] N. Marie et al., Phys. Rev. C 58 (1998) 256.
[24] M.B. Tsang et al., Phys. Rev. Lett. 78 (1997) 3836.
[25] H. Xi et al., Phys. Lett. B 431 (1998) 8.
[26] D.J. Morrissey et al., Annu. Rev. Nucl. Part. Sci. 44 (1994) 27.
[27] Y.G. Ma et al., Phys. Lett. B 390 (1997) 41.
[28] W. Bauer, Phys. Rev. C 51 (1997) 803.
[29] D. Cussol et al., Nucl. Phys. A 561 (1993) 298.
[30] M. D'Agostino et al., Nucl. Phys. A 650 (1999) 329.